Journal of Alloys and Compounds 873 (2021) 159835

Contents lists available at ScienceDirect

Journal of Alloys and Compounds

journal homepage: www.elsevier.com/locate/jalcom

Network former mixing (NFM) effects in alkali germanotellurite glasses

Henrik Bradtmüller[a,b], Ana Candida Martins Rodrigues[b], Hellmut Eckert[a,c,*]

[a] Institut für Physikalische Chemie, Westfälische Wilhelms-Universität, Corrensstr. 30, D-48149 Münster, Germany
[b] Universidade Federal de São Carlos, Departamento de Engenharia de Materiais, CP 676, 13565-905 São Carlos, SP, Brazil
[c] Instituto de Física de São Carlos, Universidade de São Paulo, Av. Trabalhador Sãocarlense 400, 13566-590 São Carlos, SP, Brazil

ARTICLE INFO

Article history:
Received 30 July 2020
Received in revised form 31 March 2021
Accepted 2 April 2021
Available online 6 April 2021

Keywords:
Tellurite glasses
Germanate glasses
Network former mixing
NFM
Solid-state NMR
Ion-conducting glasses

ABSTRACT

Network former mixing (NFM) effects on ionic conductivities have been characterized in ternary germanotellurite glasses of composition $(A_2O)_{0.3}[(TeO_2)_x(GeO_2)_{1-x}]_{0.7}$ (A = Li, Na), revealing an interesting cation dependence. While the results demonstrate a weak positive NFM effect in the Li-containing system, the electrical conductivities of the Na-containing systems correspond to the weighted average values observed in their binary endmembers. The structural origins of these differing effects have been explored by Raman scattering and ^{125}Te solid-state NMR spectroscopy, indicating no significant differences in the structural organization of these materials. Overall, the data suggest that the concentration of heteroatomic connectivities is relatively low. For the Li-containing system, an analysis of the motional narrowing effects observed in temperature-dependent static ^{7}Li NMR spectra confirms the existence of a weak positive NFM effect at the local atomic level. Accordingly, the absence of an NFM effect for the Na-containing system is corroborated by low-temperature ^{23}Na spin-echo decay spectroscopy, showing very similar network modifier distributions in those glasses.

1. Introduction

The mixing of two or several network former species is a common approach of fine-tuning combinations of relevant physical properties for a glass system towards a specific application. This approach has been particularly often used in the field of ion-conducting glasses, where successive replacement of one network former by another one at fixed mobile ion concentration can lead to significant changes in the electrical properties [1–4]. In oxide glass systems such *network former mixing effects* (NFM effects) have been characterized for most of the possible binary combinations of the network formers SiO_2, B_2O_3, P_2O_5, GeO_2, and TeO_2 for at least one level of ion concentration. A *positive* NFM effect signifies that the electrical conductivity of the ternary three-component glass is higher than the concentration-weighted average of the conductivities of its binary endmember constituents. Such behavior has been observed for borophosphate [5–10], phosphogermanate [11,12], phosphotellurite [13], tellurosilicate [14], and high-alkali borosilicate glasses [15]. Negative NFM effects have been less commonly observed. Well documented cases include low-alkali borosilicate [16,17] and alkali borotellurite glasses [18–20]. Finally, no significant network-former mixing effect was detected in an early study of borosilicate glasses [21], as well as in limited work on germanosilicate [22] and germanotellurite glasses [23].

For optimizing glass formulations for specific applications there is obviously a great need of understanding and modeling the relation between glass composition and properties on a structural basis [24–31]. Nuclear magnetic resonance (NMR) has emerged as a powerful element-selective, inherently quantitative structural method for the comprehensive characterization of NFM effects. Information extracted from NMR spectroscopy can include the identification and quantification of local network former units (NFUs) and their connectivities [4,32], the local environments and spatial distributions of the mobile ions [33], as well as the local dynamic aspects of their mobility [34].

One of the most poorly studied systems – both with regard to electrical conductivities and structural details –are the germanotellurite glasses, for which only a single composition, $(Na_2O)_{0.2}$–$(TeO_2)_{0.4}$–$(GeO_2)_{0.4}$, has been investigated so far [23]. Here we report the first systematic and comprehensive study of such glasses, namely the preparation, characterization, and ionic conductivity measurements of glasses in the systems $(A_2O)_{0.3}[(TeO_2)_x(GeO_2)_{1-x}]_{0.7}$ (A = Li, Na). These compositions present a compromise between a desired high ionic conductivity and satisfactory stability against crystallization. Structure and dynamics are explored based on detailed Raman scattering as well as

* Corresponding author at: Institut für Physikalische Chemie, Westfälische Wilhelms-Universität, Corrensstr. 30, D-48149 Münster, Germany.
E-mail addresses: eckert@ifsc.usp.br, eckerth@uni-muenster.de (H. Eckert).

https://doi.org/10.1016/j.jallcom.2021.159835
0925-8388/

solid-state ^{125}Te, ^{23}Na, and ^{7}Li NMR studies. Based on these results we will discuss the relevant composition – structure – property relations in this system.

2. Experimental

2.1. Glass preparation and characterization

Glass samples were prepared in 12 g batches by conventional melt quenching. Powder mixtures of finely ground Li_2CO_3 (Oregon L.W., 99.99%), Na_2CO_3 (Alfa Aesar 99.95–100.05%), GeO_2 (Alfa Aesar, 99.999%), and TeO_2 (Merck, 99.5%), were homogenized in a rotary jar mill for 12 h and then melted in a platinum crucible inserted in a bottom-loading high-temperature furnace. Melting temperatures varied from 780 °C to 1130 °C depending on compositions. High-GeO_2 containing glasses required higher temperatures to assure sufficiently low melt viscosities. The melting times ranged between 30 and 40 min. During the last 5 min of melting the crucible was vigorously agitated one to two times for about 30 s to homogenize the melt. Glasses were formed by *splat-quenching* the melt on a stainless-steel plate kept at room temperature. The formed glasses were then heat-treated for 12 h at an annealing temperature of T_g −30 °C to relieve thermal stress before they were slowly cooled to room temperature. Glasses were transparent with a yellowish color which became more intense in samples with higher tellurium contents. Sodium-containing glasses with high TeO_2 content ($x > 0.5$) became slightly turbid over time.

The glassy state was confirmed by X-ray diffraction, using a Rigaku Ultima IV diffractometer with Cu target (K_α wavelength) at 40 kV and 20 mA. The 10–80° 2θ range was probed at room temperature employing an integration time of 1 s and a step size of 0.02°. The results are shown in Figs. S1 and S2. Na-containing glasses with x = 0.8 and 1.0 showed weak reflections of the phase $Na_2Te_2O_5(H_2O)_2$. Their intensity increased substantially over 2 years' storage time, see also Fig. S3. Glass transition temperatures, T_g, were determined by Differential Scanning Calorimetry (DSC) using a NETZSCH, Thermische Analyse DSC 404 cell equipped with a TASC 414/3 controller. Bulk samples were ramped to high temperature with a heating rate of 10 °C/min in a platinum crucible.

Na_2O, GeO_2, and TeO_2 contents were determined semi-quantitatively on polished glass pieces by Wavelength Dispersive X-ray Fluorescence spectroscopy (WDXRF) on a ZSX PrimusII spectrometer and Energy Dispersive X-ray Spectroscopy (EDS) on a FEI (Inspect S50) Scanning Electron Microscope operated at 25 kV coupled to an energy dispersive spectroscope detector (ApolloX). For EDS, the glass specimens were sputtered unilaterally with gold for 20 s. Quantification was based on the comparison of relative element-specific emission intensities. The results are summarized in Table S1. While experimentally determined TeO_2 and GeO_2 contents are close to the batched values (within experimental errors), the Na_2O contents appear to be systematically decreased in relation to the nominal compositions. As the apparent sodium deficits tend to be higher in the Ge-rich samples (prepared at higher melting temperatures) we may attribute these deficits to melt evaporation losses. We note, however, that the low sensitivity of XRF and EDS for Na detection implies relatively low precision with which sodium contents can be determined. As the above methods do not permit any analyses for lithium content, the latter were determined by inductively coupled plasma atomic emission spectroscopy (ICP-OES) performed on a Thermo iCAP 7000 spectrometer. Before the experiments, the glass samples were completely dissolved in 50% HNO_3 within CEM MarsXpress vessels. The dissolution process was supported by microwave radiation. The results (see Table S1) reveal good agreement between nominal and experimental lithium contents.

Raman spectra were recorded with a Bruker SENTERRA Raman microscope equipped with a 785 nm laser, using 1 mW of excitation power. An objective with a 50-fold magnification and gratings of 400 grooves mm^{-1} were used. Some measurements were done with 1200 grooves mm^{-1} but did not yield an improved resolution. 10 integrations with an integration time of 60 s were used to collect the spectra. Reproducibility was ensured by collecting and averaging spectra from three different loci on each sample.

2.2. Electrical conductivity measurements

Electrical conductivities were determined under ambient conditions, using a Novocontrol Alpha A impedance analyzer equipped with a two-point cell. Bulk cylindrical samples of ~5 mm diameter and 0.7–1 mm thickness with sputtered Au electrodes on both parallel faces were measured over the frequency range 0.1 Hz to 10 MHz, and the temperature range 100 °C to T_g-30 °C. The peak-to-peak voltage value of the applied AC signal was 0.14 V, corresponding to 0.1 V RMS. All the Nyquist diagrams show a single semicircle followed by a characteristic straight line, which is due to electrode polarization. Data were multiplied by the geometrical factor S/l (S being the electrode surface area in contact with the electrolyte, and l, the thickness), thus, the resistivity (ρ) was determined from the low-frequency intercept of the semicircle with the real axis, determined by fitting a semi-circle function to the data according to:

$$y = -(y_0 + (r^2 - (x - x_0)^2)^{1/2}), \quad (1)$$

where x_0 and y_0 represent offsets on the Z' and Z'' axes respectively, and r represents the radius of the semi-circle. This method yielded equivalent results compared to the commonly used "fit semi-circle" function of the closed-source Zview software, see also Fig. S4. Ionic conductivities (σ) were then calculated from the expression, $\sigma = 1/\rho$, respectively. The activation energy $E_A\sigma$ of ion conduction was extracted from the slope of the Arrhenius plot of log $\sigma_{DC}T$ vs. $10^3/T$ based on the expression,

$$\sigma_{DC}T = \sigma_0 \exp(-E_A^{\sigma}/RT) \quad (2)$$

2.3. Solid-state NMR spectroscopy

An Agilent DD2 spectrometer interfaced with a 5.64 T magnet (^{1}H frequency at 243 MHz) and equipped with a triple-channel 4 mm NMR probe was used for the solid-state NMR experiments. Static ^{125}Te NMR spectra were measured at room temperature, using wideband-uniform rate-smooth truncation (WURST) pulses in a Carr-Purcell-Meiboom-Gill (CPMG) sequence [35,36]. With WURST pulse lengths of 50.0 μs, an excitation bandwidth of 500 kHz, and the most commonly used shape parameter of N = 80, the excitation window was found to be sufficiently broad to record the whole spectra, thus not requiring a carrier frequency stepped approach. Identical WURST excitation and refocusing pulses were used. The signal-to-noise ratios were enhanced by co-adding 64 echoes produced via the CPMG pulse sequence. Recycle delays were 40–100 s. Frequency-domain spectra were obtained by fast Fourier transformation of the co-added echoes. ^{125}Te chemical shifts are reported relative to the resonance line of crystalline CdTe. ^{7}Li and ^{23}Na MAS NMR spectra were measured on a Bruker DSX 500 spectrometer in a 4 mm MAS-NMR probe operated at a spinning frequency of 14.0 kHz, using short pulses of 0.3–0.4 μs length and relaxation delays of 2.0 and 0.5 s, respectively. Chemical shifts are reported relative to 0.1 M aqueous LiCl and NaCl solutions.

Static ^{7}Li NMR experiments were done on the Agilent spectrometer using a commercial triple channel 4 mm probe operated at temperatures between 173 and 473 K. Single-pulse experiments employed pulse lengths of 2.75 μs with relaxation delays between 2 and 20 s. Experimental spectra were analyzed using mixed Gaussian/

Table 1
Employed melting temperatures (T_{m^*}), measured glass transition (T_g) and crystallization (T_x) temperatures, logarithmic DC-electrical conductivities extrapolated to 293 K (log (σ_{293K})), activation energies (E_A^σ), and the logarithm of the pre-exponential factor (log(σ_0)) of Eq. (2) in $(A_2O)_{0.3}[(TeO_2)_x(GeO_2)_{1-x}]_{0.7}$ (A = Li, Na) glasses.

Composition		T_{m^*}/K	T_g/K	T_x/K	log (σ_{293K} / $\Omega^{-1}cm^{-1}$)	E_A^σ/ ±0.01 eV	log (σ_0/k$\Omega^{-1}cm^{-1}$)
M = Li	x = 0.0	1403	749	829	−9.99	0.79	6.06
	x = 0.2	1373	683	771	−10.69	0.80	5.58
	x = 0.4	1173	634	743	−11.04	0.83	5.71
	x = 0.5	1173	607	746	−11.09	0.84	5.86
	x = 0.6	1098	585	756	−11.19	0.83	5.63
	x = 0.8	1053	548	693	−11.90	0.90	6.03
	x = 1.0	1053	520	583	−12.42	0.93	6.02
M = Na	x = 0.0	1333	745	829	−9.92	0.71	4.82
	x = 0.2	1373	680	747	−10.76	0.79	5.22
	x = 0.4	1173	600	711	−11.27	0.83	5.40
	x = 0.5	1173	573	694	−11.88	0.87	5.60
	x = 0.6	1123	543	700	−12.19	0.90	5.68
	x = 0.8	1053	514	678	−12.57	0.90	5.46
	x = 1.0	1053	498	571	−13.74	0.98	5.66

Lorentzian line shape functions to extract the full width at half maximum of the spectra. All data processing and parameter extraction was done using the DMFIT software [37]. For measuring the strength of homonuclear ^{23}Na–^{23}Na dipole-dipole interactions static Hahn spin-echo (90°–τ_1 – 180°–τ_1) decays were recorded on a Bruker Avance 400 MHz spectrometer, at 173 K, using 90° and 180° pulse lengths of 8.3 and 16.7 µs and a relaxation delay of 2 s. Data were analyzed in terms of Gaussian decays over dipolar evolution times up to $2\tau_1$ = 200 µs, where the decays could be approximated as Gaussians, according to the expression [38]:

$$I(2\tau_1)/I(0) = \exp(-M_{2(\mathrm{Na\text{-}Na})}/2\ (2\tau_1)^2) \quad (3)$$

For each sample at least two independent measurements were obtained and the resulting M_2 values averaged.

3. Results and interpretation

3.1. Glass properties

Table 1 summarizes the compositions and bulk properties of the glasses examined and the chemical analysis data is summarized in Table S1 in the Supporting Materials Section. In both systems, T_g decreases with increasing tellurium oxide content in a non-linear fashion. Fig. 1 summarizes the Arrhenius plots derived from temperature-dependent electrical conductivity measurements. Representative Nyquist diagrams from which the electrical resistivities were extracted are shown in Fig. S6 of the Supporting Materials Section. To examine the existence of a positive or negative network former mixing effect, it is customary to plot the ionic conductivity at a fixed temperature and the activation energy, E_A^σ, against the compositional parameter *x* determining the network former inventory. A positive effect exists if the ionic conductivity is higher and the activation energy of ion conduction is lower than the value obtained by linear interpolation of the values obtained for the single network former glasses having the endmember compositions. Fig. 2 shows these plots for the ionic conductivity extrapolated to room temperature and for the activation energies. We detect a small positive network former mixing effect for the Li-containing glasses, whereas no network former mixing effect is detectable for the Na-containing glasses. To the best of our knowledge, this is the first time that lithium and sodium-containing glasses behave differently in a mixed network former glass system. We note, however, that we cannot exclude the possibility that the detection of a positive network former mixing effect has been obscured in the present study by the apparent variations in actual sodium contents. On the other hand, we do not observe a systematic influence of the apparent Na losses on the ionic conductivities measured, i.e., those samples in which the chemical analysis suggests particularly high Na losses do not necessarily show particularly strongly decreased electrical conductivities.

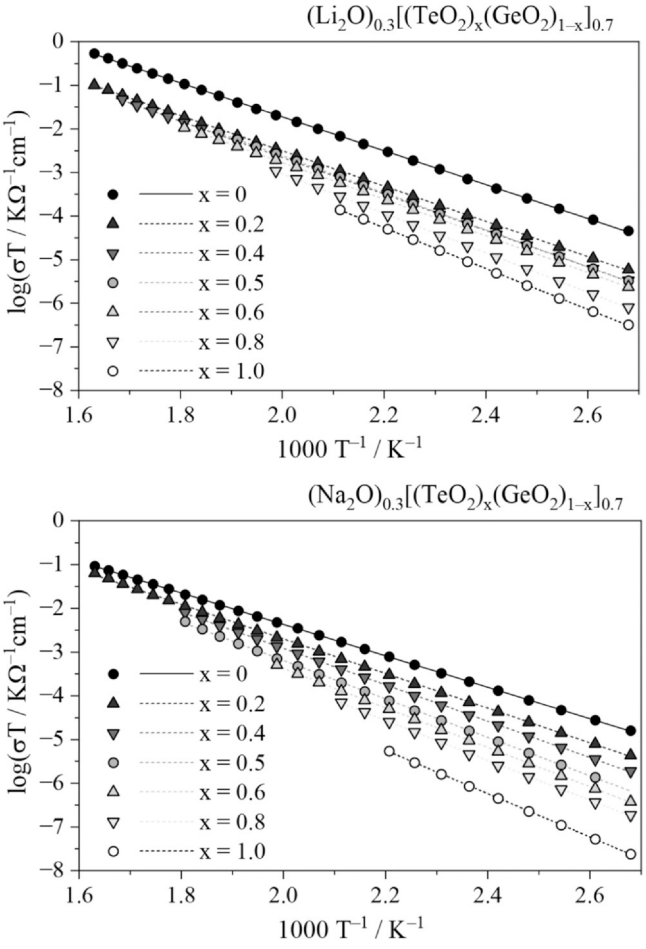

Fig. 1. Temperature-dependent electrical conductivities in $(A_2O)_{0.3}[(TeO_2)_x(GeO_2)_{1-x}]_{0.7}$ (A = Li, Na) glasses and linear fits to Eq. (2) (solid and broken lines).

3.2. Raman spectra

Fig. 3 shows the Raman spectra for both systems. Results are completely analogous for the lithium- and sodium-based glasses and can be interpreted jointly, even though the spectra of the Na-containing glasses are considerably better resolved. The Raman spectra of the high-germanium glasses are dominated by a broad, asymmetric feature with a

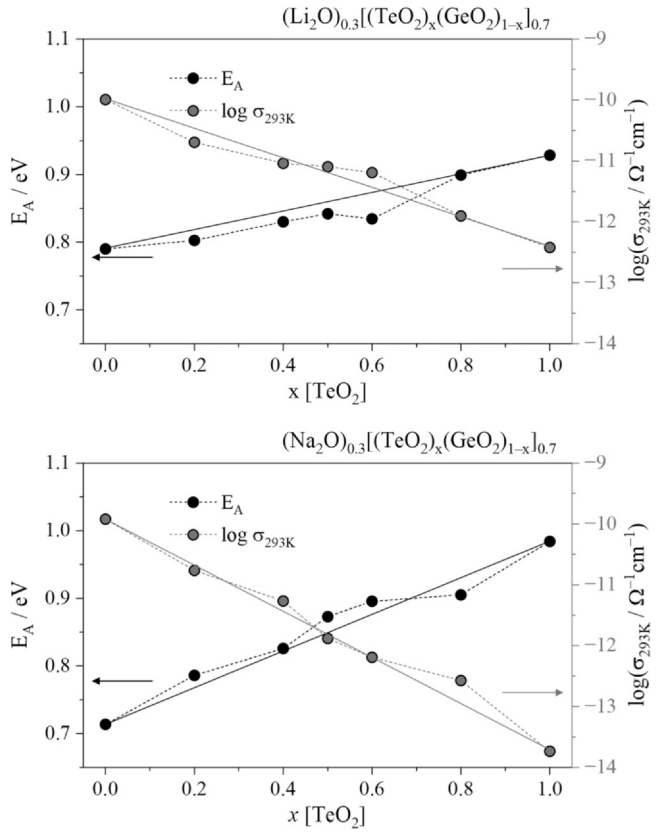

Fig. 2. Logarithmic, DC-electrical conductivities σ at 293 K and activation energies of ion conduction in $(A_2O)_{0.3}[(TeO_2)_x(GeO_2)_{1-x}]_{0.7}$ (A = Li, Na) glasses. Experimental errors correspond to symbol sizes. Black and gray solid lines connect the endmember samples serving as a guide to the eye concerning NFM effects.

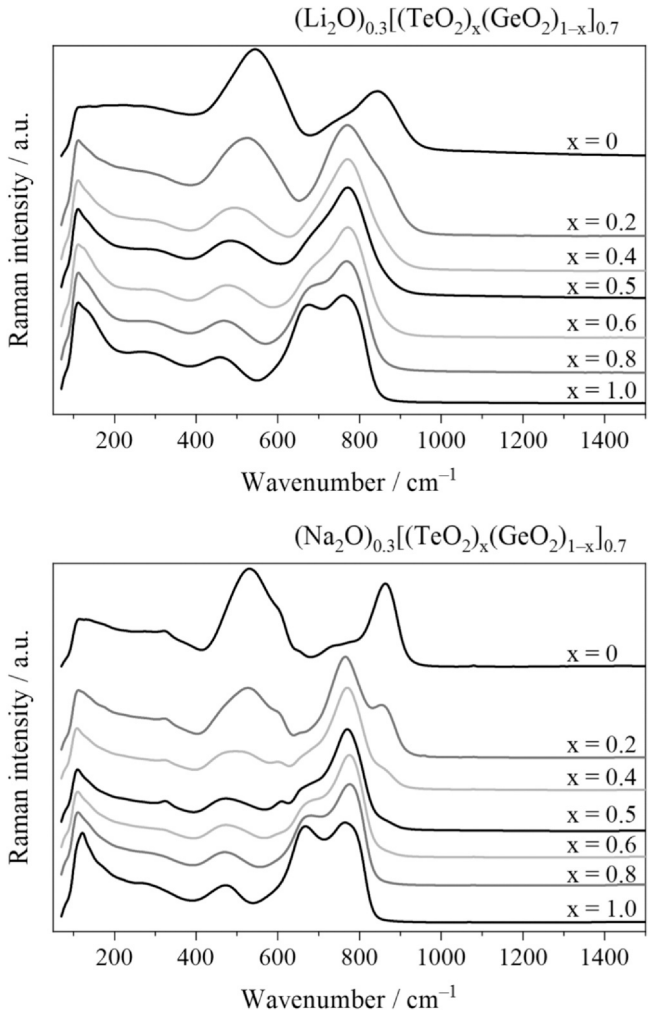

Fig. 3. Raman spectra of $(A_2O)_{0.3}[(TeO_2)_x(GeO_2)_{1-x}]_{0.7}$ (A = Li, Na) glasses.

maximum near 500 cm^{-1}, which can be attributed to the Ge–O–Ge network vibrations, including the symmetric vibrations of four- and three-membered germanate rings at ~425 and ~525 cm^{-1}, respectively. In the Na-containing system, the spectra are somewhat better resolved, allowing identification of a separate band near 580 cm^{-1}. In addition, in the binary germanate glass, the most intense bands are observed at 750 and 870 cm^{-1}. The binary germanate glasses show appreciable intensity in the 600–650 cm^{-1} region usually attributed to Ge-O linkages in octahedrally coordinated Ge [39], suggesting that these units do occur in these samples. The bands at 750 and 870 cm^{-1} are assigned to (GeO_2) stretch;sym and (GeO)stretch;sym modes, indicating the presence of non-bridging oxygens associated with Ge^2 and Ge^3 units, respectively. In the terminology used here, the superscript identifies the number of bridging oxygen atoms linked to the NFU. While the band near 750 cm^{-1} is strongly overlapped by scattering signals originating from the tellurite component, the band at 870 cm^{-1}, attributable to Ge^3 units, can be observed up to $x = 0.4$ in both systems. Starting already at rather low Te-contents, the Raman spectra are increasingly dominated by the scattering of the tellurium containing NFUs. Consistent with previous results on binary alkali tellurite glasses [40,41], we attribute bands near 460, 670, and 760 cm^{-1} to vibrations involving the tellurite NFUs. As suggested in these earlier works the band near 670 cm^{-1} may be assigned to asymmetric Te–O stretching modes of four-coordinate tellurium. The band near 760 cm^{-1} reflects vibrations of non-bridging oxygen atoms associated with three-coordinate units [40,41]. Fig. 3 shows a systematic evolution in the spectra, suggesting that the ratio of four-coordinate to three-coordinate tellurium-based NFUs increases systematically with increasing TeO_2 content. Finally, the band near 460 cm^{-1} is also observed in binary alkali tellurite glasses and is believed to be due to vibrations of bridging oxygen atoms within Te–O–Te linkages. Interestingly, this band is already strongly observable in our ternary glasses at rather low Te contents ($x = 0.2$), suggesting the presence of such linkages already in this composition range. This finding may be some evidence of partial segregation effects. Finally, the Raman spectra do not show any scattering peaks that do not appear in the binary glasses. Thus, Fig. 3 shows no spectroscopic evidence for Ge–O–Te linkages. It is clear, however, that failure of observing distinct spectroscopic features signifying such linkages should not be taken as proof of their absences.

3.3. ^{125}Te NMR

Fig. 4 shows ^{125}Te WURST-CPMG NMR spectra obtained by Fourier transformation of the sum of the individual spin-echoes ("envelope" spectra – black curves) of the glasses and of crystalline α-TeO_2. While the dominant interaction affecting the lineshapes appears to be the chemical shift anisotropy (CSA), the spectra of the glasses, unlike the one of crystalline α-TeO_2, cannot be described by a unique set of principal tensor components. This situation may be attributed to the amorphous character of the glasses, in which there is likely a distribution of Te-O bond distances and O-Te-O as well as Te-O-Te bond angles that are expected to lead to a distribution of chemical shift tensor components. Indeed, the spectra of the glasses can be simulated using Gaussian distributions of the three principal magnetic shielding parameters, following the approach published previously [20]. Table 2 summarizes the average values of the isotropic chemical shifts δ_{iso} and the principal tensor components δ_{xx}, δ_{yy}, and δ_{zz}, as well as their Gaussian distribution widths χ_{ii}. The results show very little variation in the ^{125}Te NMR spectra as a

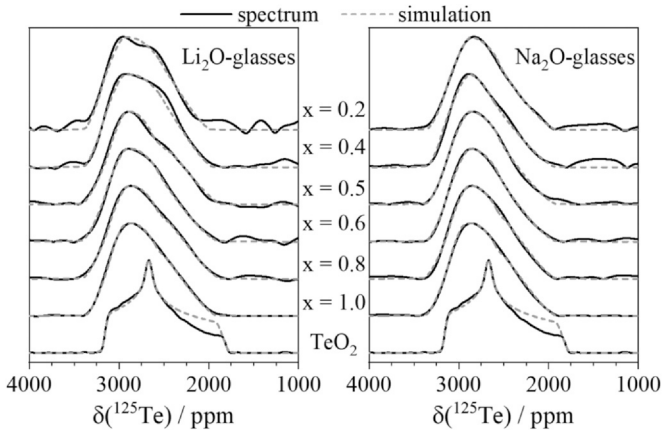

Fig. 4. ^{125}Te solid-state NMR spectra of $(A_2O)_{0.3}[(TeO_2)_x(GeO_2)_{1-x}]_{0.7}$ (A = Li, Na) glasses (M = Li, Na) and of α-TeO_2. Chemical shifts are referenced to crystalline CdTe. Gray, dashed lines represent simulations assuming different Gaussian distributions of the three principle magnetic shielding parameters (see ^{125}Te NMR section).

Table 2
Average chemical shift tensor parameters (in ppm, ± 50 ppm) obtained from the spectral deconvolution of the ^{125}Te WURST-CPMG spectra. Time-domain data of all experiments have been apodized by a Gaussian window function, with a corresponding *FWHM* of 1 ppm in the frequency domain.

	x (TeO_2)	δ_{xx}	δ_{yy}	δ_{zz}	χ^{xx}	χ^{yy}	χ^{zz}	δ_{iso} (±10)
α-TeO_2		3160	2670	1850	70	55	130	2560
M = Li	0.2	3170	2880	2260	400	650	520	2770
	0.4	3170	2860	2240	400	650	520	2760
	0.5	3170	2870	2140	450	450	520	2730
	0.6	3170	2860	2230	450	570	630	2750
	0.8	3160	2850	2160	450	510	530	2720
	1.0	3160	2850	2200	380	490	530	2740
M = Na	0.2	3110	2860	2250	450	580	630	2740
	0.4	3110	2920	2260	450	560	630	2760
	0.5	3120	2860	2250	450	570	630	2740
	0.6	3120	2860	2250	450	570	630	2740
	0.8	3140	2850	2200	450	510	530	2730
	1.0	3160	2850	2200	380	490	530	2740

function of composition, in contrast to the continuous evolution of the part of the Raman spectra associated with the Te-O stretching modes active for the TeO_3 and TeO_4 NFU-s. It appears that the ^{125}Te magnetic shielding parameters in this system are unable to differentiate between three- and four-coordinate tellurium species. A similar result was previously observed in lithium and sodium borotellurite glasses [19,20], and may also be related to the noted indistinguishability of bridging and non-bridging oxygen species by ^{17}O NMR and X-ray photoelectron spectroscopy [42]. However, whereas for the borotellurite glass system a weak but monotonic dependence of the average ^{125}Te isotropic chemical shifts on the Te/B ratio could still be detected, the corresponding data for the present glass system do not show any dependence on the glass network composition within experimental error. Thus, our ^{125}Te NMR data are consistent with an even lower level of Ge-O-Te linkages in the present glasses than the level of B-O-Te linkages in the borotellurite glass system. Consistent with the Raman spectroscopic data, the ^{125}Te NMR spectra also do not give any positive evidence of Ge-O-Te linkages. Possibly these methods are not very sensitive to Ge-O-Te versus Te-O-Te linking, as the crystal structure of $GeTe_2O_6$ reveals that the Ge-O and Te-O bond lengths (187 pm) are close to identical [43]. On the other hand, the data are also consistent with a nanoscale segregation model into non-connected germanate and tellurite domains.

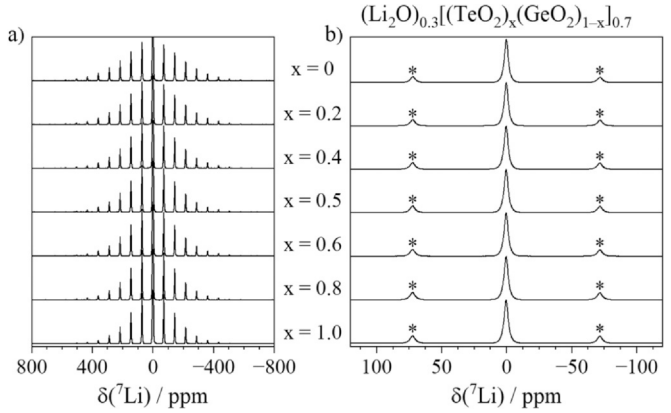

Fig. 5. (a) Full ^{7}Li MAS NMR spectra of $(Li_2O)_{0.3}[(TeO_2)_x(GeO_2)_{1-x}]_{0.7}$ glasses. The central transition signal is truncated to emphasize the spinning sideband intensity profile. (b) Sections of (a), showing the non-truncated central transition and the first set of spinning sidebands (marked by asterisks).

3.4. ^{7}Li and ^{23}Na MAS-NMR

^{7}Li MAS-NMR spectra measured on the Li-containing glasses (Fig. 5) reveal a sharp central m = ½ <–> m = ⁻½ transition which could be modeled as Gauss/Lorentz curves, having a chemical shift near 0.4 ± 0.1 ppm and a linewidth of 3.6 ± 0.1 ppm independent of composition (see Table 4). It is flanked by wide spinning sideband patterns associated with the non-central m = ±½ <–> m = ±3/2 transitions that are broadened inhomogeneously due to the anisotropy of the quadrupolar interactions. The frequency range over which these sidebands extend, decreases slightly, indicating a slight reduction of the average ^{7}Li quadrupolar coupling constant with increasing *x*. Fig. 6 shows the ^{23}Na MAS-NMR spectra of the sodium-containing glasses. We observe the typical asymmetric lineshape for nuclei affected by second-order quadrupolar broadening and a wide distribution of electric field gradients [44]. Using the *Czjzek simple* model [44] in the *DMfit* software [37], average values for the isotropic chemical shifts δ_{iso}^{cs} and the second-order quadrupolar effect ($SOQE = C_Q(1+\eta_Q^2/3)^{1/2}$) can be obtained via simulation of these spectra. In the foregoing expression, C_Q and η_Q represent the nuclear electric quadrupolar coupling constant and the electric field gradient asymmetry parameter, respectively. ^{23}Na chemical shifts of the binary sodium germanate and sodium tellurite glasses are consistent with those reported previously [19,33,45]. Table 3 indicates a monotonic, (albeit non-linear) increase in the ^{23}Na isotropic

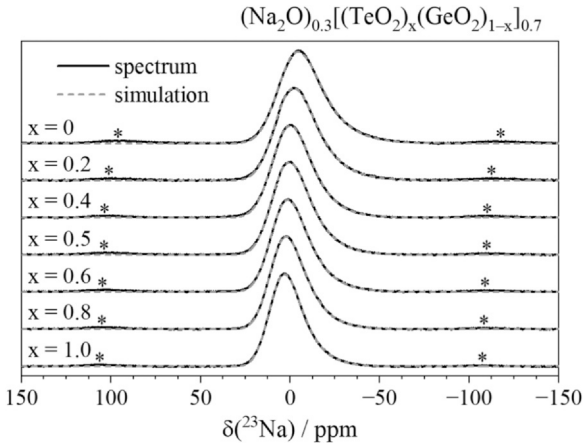

Fig. 6. ^{23}Na MAS NMR spectra of $(Na_2O)_{0.3}[(TeO_2)_x(GeO_2)_{1-x}]_{0.7}$ glasses and their lineshape simulations using the *Czjzek* distribution model (dashed gray lines). Asterisks mark spinning sidebands.

Table 3
NMR parameters obtained from the lineshape analysis of the ^{7}Li MAS NMR spectra (chemical shift δ_{iso}^{cs} and full width at half maximum, *FWHM*) and the simulations of the ^{23}Na MAS NMR spectra shown in Fig. 6 (average isotropic chemical shift, δ_{CS}^{iso}, and the average *SOQE* parameter).

x (TeO_2)	(^{7}Li) δ_{iso}^{cs}/ppm ±0.2 ppm	(^{7}Li) *FWHM*/ppm ±0.2 ppm	(^{23}Na) δ_{CS}^{iso}/ppm ±0.2 ppm	(^{23}Na) *SOQE*/MHz ±0.1 MHz
0	0.4	3.4	5.5	2.9
0.2	0.5	3.5	7.4	2.8
0.4	0.6	3.7	8.5	2.6
0.5	0.4	3.6	9.0	2.7
0.6	0.2	3.7	9.8	2.7
0.8	0.5	3.7	10.4	2.6
1.0	0.3	3.6	10.6	2.5

Table 4
^{23}Na homonuclear dipole-dipole second moments $M_{2(Na\text{-}Na)}$ (in units of 10^{6} rad^{2}s^{-2} ±10%) of $(Na_2O)_{0.3}[(TeO_2)_x(GeO_2)_{1-x}]_{0.7}$ glasses.

x (TeO_2)	0	0.2	0.4	0.5	0.6	0.8	1.0
$M_{2(Na\text{-}Na)}$	2.25	2.63	2.50	2.35	2.17	3.50	2.52

chemical shift, and a monotonic decrease of the *SOQE* values, reflecting the successive replacement of anionic germanium-based units by anionic tellurium-based units in the vicinity of the sodium ions with increasing x-value. These trends do not suggest any particular preference of sodium ions interacting with one of the two network former components, and thus can be considered consistent with a proportional sharing model.

3.5. ^{23}Na static spin-echo decay spectroscopy

Inferences about the spatial distribution of the sodium ions can be drawn from ^{23}Na spin-echo decay spectroscopy [38]. This experiment is sensitive to the homonuclear ^{23}Na–^{23}Na magnetic dipole-dipole coupling strength, which is described in terms of the dipolar second moment $M_{2(Na\text{-}Na)}$ and obtained by analyzing the decay of echo amplitude versus the dipolar evolution time $2\tau_1$ in terms of Eq. (3). Fig. 7 summarizes the results. It is noted that, for clarity, the echo decay intensity is plotted in a semi-logarithmic fashion as $\ln(I/I_0)$ against $(2\tau_1)^2$, thus enabling a straightforward analysis of the Gaussian decays by linear regressions. As found in previous studies, strictly Gaussian behavior is only found within a limited data range and the analysis in terms of Eq. (3) has been restricted to the regime ($0 < 2\tau_1 < 200$ µs). The bottom part of Fig. 7 shows the compositional dependence of $M_{2(Na\text{-}Na)}$ determined in this fashion. As indicated by Table 4, values in the vicinity of 2.5×10^{-6} rad^2/s^2 are found.

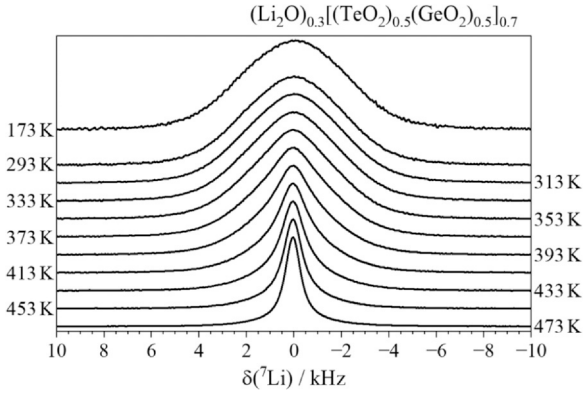

Fig. 8. ^{7}Li static NMR spectra for the glass sample $(Li_2O)_{0.3}[(TeO_2)_{0.5}(GeO_2)_{0.5}]_{0.7}$ measured as a function of temperature.

The data for the binary endmember glasses are similar to those previously published by us [33], however, our value for $(Na_2O)_{0.3}(TeO_2)_{0.7}$ is significantly smaller than the one found for this composition in reference [46]. For the ternary mixed-network glasses the $M_{2(Na\text{-}Na)}$ values are constant within experimental error. Altogether, when compared to $M_{2(Na\text{-}Na)}$ values in other binary and ternary glass systems [19,33] these data are consistent with a random spatial distribution of the sodium ions. Also, the monotonic dependence of $M_{2(Na\text{-}Na)}$ on network former composition is consistent with the documented absence of NFM effects in this Na-containing glass system. A significant deviation can be observed for the $x = 0.8$ sample, which may arise from some clustering or phase separation.

3.6. Variable temperature ^{7}Li static NMR

In order to investigate the Li^+ ionic mobility in the studied glasses, static variable temperature ^{7}Li NMR experiments were performed. Fig. 8 shows a representative set of ^{7}Li NMR spectra for the sample with $x = 0.5$.

Fig. 9 (top) shows that the derived *FWHM* values at low temperature, which are dominated by the homonuclear ^{7}Li-^{7}Li magnetic dipole-dipole interactions, are essentially independent of x, indicating that the spatial distributions of the lithium ions are very similar in these glasses. When increasing the temperature, the line widths become narrower due to the motional averaging of the magnetic dipole-dipole interactions as the inverse motional correlation time, $1/\tau_c$, becomes comparable to the respective rigid lattice line widths in rad/s. At sufficiently high temperatures, the static linewidth reaches an approximately constant plateau value of

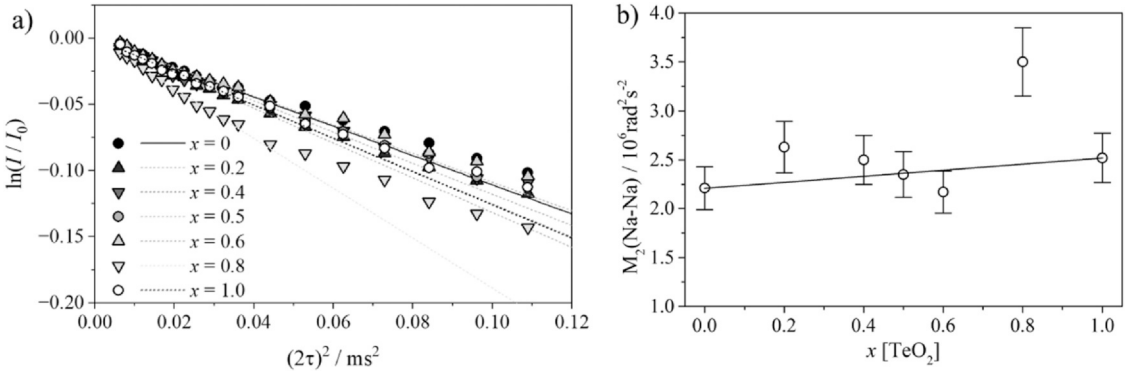

Fig. 7. (a) ^{23}Na spin-echo decays of $(Na_2O)_{0.3}[(TeO_2)_x(GeO_2)_{1-x}]_{0.7}$ glasses. Solid lines depict least-squares fits to Eq. (3) in a semi-logarithmic form within the data range ($0 < 2\tau_1 < 200$ µs). b): Second moments $M_{2(Na\text{-}Na)}$ (in units of 10^{6} rad^{2}s^{-2} ±10%) of $(Na_2O)_{0.3}[(TeO_2)_x(GeO_2)_{1-x}]_{0.7}$ glasses. The solid line is an interpolation between the data obtained for the binary endmember glasses and serves as a guide to the eye.

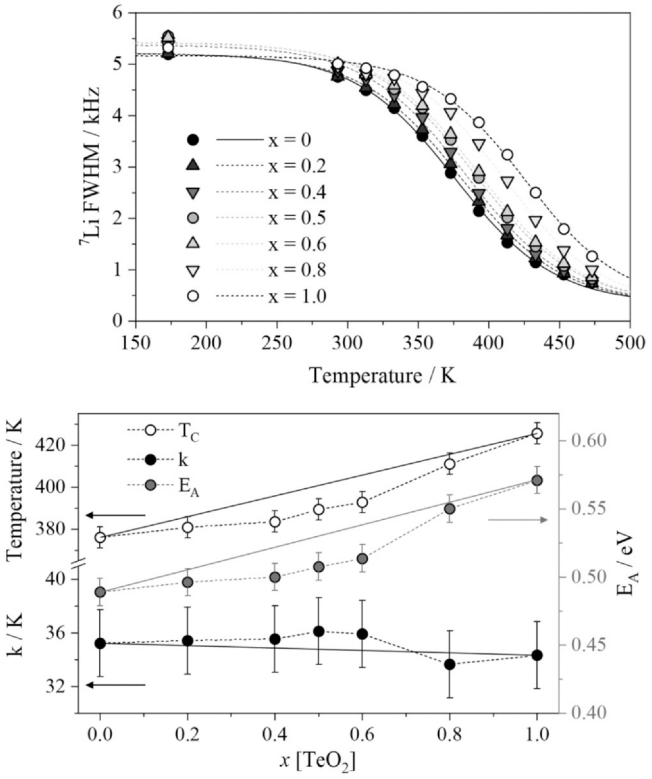

Fig. 9. (a) Full-width at half-maximum of the static ^{7}Li NMR spectra as a function of composition and temperature for glasses in the system $(Li_2O)_{0.3}[(TeO_2)_x(GeO_2)_{1-x}]_{0.7}$. (b) Values of the critical temperature T_C, k, and E_A^{NMR}, obtained by fitting the curves in (a) to Eqs. (4) and (5), as a function of composition. Black and gray solid lines connect the endmember samples serving as a guide to the eye concerning NFM effects.

0.34 kHz. Fig. 9 (top) summarizes the results for the whole set of investigated samples. The curves can be described by two plateaus separated by a relatively narrow temperature range where the change in linewidth occurs.

As previously discussed [20], this motional narrowing process can be modeled phenomenologically, using the empirical equation [47],

$$FWHM(T) = \frac{F_0}{1 + e^{\frac{(T-T_C)}{k}}} + F_\infty, \quad (4)$$

where F_0 is the difference between the two plateau values of the *FWHM*, F_∞ is the plateau value of the *FWHM* reached in the limit of sufficiently high temperatures, T_C is the temperature at the inflection point of the curve (critical temperature) and k is a parameter that characterizes the steepness of the linewidth variation. Conceptually, in glasses one expects a distribution of correlation times owing to the local variations in the depths of the energy wells defining the Li^+ local environments and thus a distribution of local mobilities, resulting in a less steep linewidth variation as a function of temperature. Thus, Eq. (4) offers the possibility of characterizing this *dynamic heterogeneity* via the parameter k on a comparative basis without knowing the exact form of the distribution function. The best-fit curves to the experimental data are shown in Fig. 9 (top) and the fitting parameters are summarized in Table 5. Fig. 9 (bottom) shows plots of the temperatures T_C as a function of the glass composition x. Consistent with the weak positive NFM effect in the E_A^σ values from c values from the electrical conductivity data, we also observe a weak positive effect in the present NMR data.

For semi-quantitative analysis, the Waugh-Fedin equation [48],

$$E_A^{NMR}\,[eV] = T_{onset}\,[K] \times 0.0016, \quad (5)$$

Table 5
Fitting parameters for the ^{7}Li motional narrowing curves using Eq. (4) and activation energies calculated via the Waugh-Fedin equation according to Eq. (5).

x (TeO_2)	F_0/kHz (±0.1)	F_∞/kHz	T_C /K (±5)	k/K (±2)	E_A^{NMR}/eV (±1 × 10^{-2})
0	4.9	0.34	376	35	0.49
0.2	4.9	0.34	381	35	0.50
0.4	5.1	0.34	384	36	0.50
0.5	5.1	0.34	389	36	0.51
0.6	5.1	0.34	393	36	0.51
0.8	4.9	0.34	411	34	0.55
1.0	4.9	0.34	426	34	0.57

has been frequently used to estimate the activation energy associated with the motional narrowing process. In this expression, T_{onset} is the onset temperature at which the second moment (or the *FWHM*) of the NMR spectrum starts to decrease as a function of temperature. Following our previous approach [20] we define it as the temperature where the low-temperature plateau line intersects with the tangent at the inflection point. The activation energies E_A^{NMR} estimated in this fashion are summarized in Table 5. They characterize local ionic hopping motions and are expected to be lower than the activation energy values E_A^σ obtained for the ionic conductivity by impedance spectroscopy, which characterize long-range transport. Nevertheless, a positive NFM effect is clearly observed by both observables (E_A^{NMR} and E_A^σ). This result indicates that the non-linear dependence of the electrical conductivity (measured by impedance spectroscopy) on composition is a direct reflection of corresponding effects upon the ionic mobilities (as measured by ^{7}Li NMR), suggesting that the modification of ionic long-range transport properties is directly related to the structural changes encountered in the local ionic environments. Furthermore, the k values are very similar for all the glasses, indicating that the dynamic heterogeneities in this series of glasses are comparable. In principle, similar motional narrowing behavior may be observable in static temperature-dependent ^{23}Na NMR spectra. However, as already indicated by the values of the electrical conductivities, the mobilities of the sodium ions in this glass system are significantly lower, shifting the motional narrowing regime into a higher-temperature region not accessible to our equipment.

4. Discussion and conclusions

Fig. 10 summarizes the current state of the literature with regard to network former mixing (NFM) effects in ternary lithium and sodium ion-conducting oxide glasses [4–23]. Positive, absent, and negative NFM effects are shown in green, yellow, and red colors, respectively. Glass compositions are represented in terms of $(A_2O)_x$–$(M_2O_4$–$M'_2O_y)_{1-x}$ (A = Li, Na; $y = 4$ for M, M' = Si, Ge, Te; $y = 3$ for M, M' = B, and $y = 5$ for M, M' = P) under continuous variation of the M/M' ratio. Additional data in the literature with glass compositions along the lines $(A_2O)_x$–$(MO_2$–$M'_2O_y)_{1-x}$ show basically the same trends. The figure shows that positive NFM effects dominate, particularly if one of the components involved is P_2O_5. Among the various ternary oxide systems investigated so far, the borotellurite glass system is the only one showing a clear negative NFM effect, whereas in borosilicate glasses, the sign of the effect depends on the cation content. Previous structural work using solid-state NMR has convincingly shown that positive NFM effects can be linked to a favorable interaction between the different network former units, resulting in the formation of new intermediate-range order configurations that serve to disperse local charges [4,49–51]. This effect produces Coulombic potential wells that are more shallow than found in the single-network former glasses, thereby enhancing ionic mobility. On the other hand, absent or negative effects are observed if such interactions do either not take place or do not open up new possibilities for favorable charge dispersal, which is the situation in the alkali

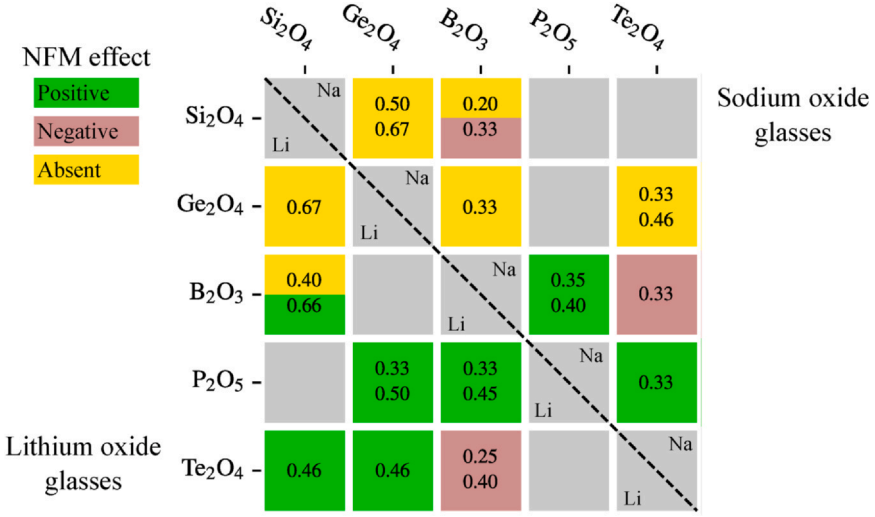

Fig. 10. Overview of the pseudo-binary oxide glass systems for which network former mixing (NFM) effects have been documented in the literature. Sodium-containing glass systems are shown above, lithium-containing systems below the diagonal. Positive effects are indicated by green, absent effects by yellow, and negative effects by red color. The network modifier concentrations (x) are indicated with respect to the glass formulation $(A_2O)_x$–$(M_2O_4$–$M'_2O_y)_{1-x}$ (A = Li, Na; $y = 4$ for M, M' = Si, Ge, Te; $y = 3$ for M, M' = B, and $y = 5$ for M, M' = P), under continuous variation of the M'/M ratio. (For interpretation of the references to color in this figure legend, the reader is referred to the web version of this article.)

borotellurite glass systems. In the latter case, we previously suggested that the negative NFM effects could occur as a result of local segregation and/or incipient phase separation phenomena.

For the germanotellurite glass system studied in the present contribution, neither Raman scattering nor ^{125}Te solid-state NMR can provide any clear evidence for mixed Ge-O-Te connectivities, even though they do not disprove their existence. Nevertheless, a weak positive NFM effect is observed for the lithium-containing system. Based on this situation we can conclude that the mere absence of proof for heteroatomic linking in the network structure alone does not necessarily allow a prediction of the sign. In other words, a positive NFM effect can still be observed even if structural work gives no evidence for heteroatomic connectivity, as in the present case.

Finally, previous work on ion-conducting mixed-network former glasses has indicated that sodium- and lithium-containing glasses having the same compositional makeup usually behave analogously. In this respect the present germanotellurite system is unique: while the sodium-containing glasses appear to show no NFM effect at all within the experimental error limits, it is positive in the lithium-containing glass system, both for the electrical conductivity and the local mobilities probed by NMR. The difference in the behavior of the sodium and lithium germanotellurite glass systems of the present contribution may be related to the length scale of segregation/phase separation phenomena involved. In this respect, the observation made in Fig. 3, that the Raman spectra of the sodium-containing glasses show a much clearer definition of the various bands identifying the separate single-network former units than those of the lithium-containing glasses, may be significant. It may indicate that the segregation phenomena in the sodium-containing system occur over a wider distance range than in the lithium-containing system. To examine this possibility, it will be worthwhile examining the NFM effects in some macroscopically phase-separated glass systems.

CRediT authorship contribution statement

HB carried out all the experimental work and the data analysis. **ACMR** supervised the electrical conductivity studies. **HE** conceptualized and supervised the spectroscopic characterization work. All authors participated in the writing of the manuscript and the preparation of the figures.

Declaration of Competing Interest

The authors declare that they have no known competing financial interests or personal relationships that could have appeared to influence the work reported in this paper.

Acknowledgments

HB is grateful for support from the São Paulo Research Foundation (FAPESP) (grant number 2019/26399-3), as well as the Deutsche Forschungsgemeinschaft (DFG). The authors would like to thank the Laboratory of Structural Characterization of the Materials Engineering Department (LCE/DEMa/UFSCar) and the Center for Research, Technology and Education in Vitreous Materials (CeRTEV), both part of the Federal University of São Carlos, for the lab facilities (grants: 2013/07793-6 and 2013/17071-8, CEPID programme, FAPESP). Finally, Rafael Bonacin de Oliveira is kindly acknowledged for his support and helpful discussions concerning the use of the XRF spectrometer.

Appendix A. Supporting information

Supplementary data associated with this article can be found in the online version at doi:10.1016/j.jallcom.2021.159835.

References

[1] T. Tsuchiya, T. Moriya, Anomalous behavior of physical and electrical properties in borophosphate glasses containing R_2O and V_2O_5, J. Non-Cryst. Solids 38–39 (1980) 323–329.
[2] R.V. Salodkar, V.K. Deshpande, K. Singh, Enhancement of the ionic conductivity of lithium borophosphate glass: a mixed glass former approach, J. Power Sources 25 (1989) 257–263.
[3] V.K. Deshpande, A. Pradel, M. Ribes, The mixed glass former effect in the Li_2S:SiS_2:GeS_2 system, Mater. Res. Bull. 23 (1988) 379–384.
[4] H. Eckert, Network former mixing (NFM) effects in ion-conducting glasses. Structure/property correlations studied by modern solid-state NMR techniques, Diffus. Found. 6 (2015) 144–193.
[5] A. Magistris, G. Chiodelli, M. Villa, Lithium borophosphate vitreous electrolytes, J. Power Sources 14 (1985) 87–91.
[6] S. Kumar, P. Vinatier, A. Levasseur, K.J. Rao, Investigations of structure and transport in lithium and silver borophosphate glasses, J. Solid State Chem. 177 (2004) 1723–1727.
[7] P.S. Anantha, K. Hariharan, Structure and ionic transport studies of sodium borophosphate glassy system, Mater. Chem. Phys. 89 (2005) 428–437.

[8] D. Zielniok, C. Cramer, H. Eckert, Structure/property correlations in ion-conducting mixed network former glasses: solid state NMR studies of the system Na_2O-B_2O_3-P_2O_5, Chem. Mater. 19 (2007) 3162–3170.

[9] R. Christensen, G. Olson, S.W. Martin, Ionic conductivity of the mixed glass former 0.35 Na_2O+0.65(xB_2O_3 + (1-x)P_2O_5) glasses, J. Phys. Chem. B 117 (2013) 16577–16586.

[10] M. Storek, R. Böhmer, S.W. Martin, D. Larink, H. Eckert, NMR and conductivity studies of the mixed glass-former effect in lithium borophosphate glasses, J. Chem. Phys. 137 (2012) 124507.

[11] K. Sklepic, R.D. Banhatti, G. Tricot, P. Mošner, L. Koudelka, A. Moguš-Milankovicantic, Insights from local network structures and localized diffusion on the ease of lithium ion transport in two mixed glass-former systems, J. Phys. Chem. C 121 (2017) 17641–17657.

[12] S. Kumar, K.J. Rao, Lithium ion transport in germanophosphate glasses, Solid State Ion. 170 (2004) 191–199.

[13] D. Larink, M.T. Rinke, H. Eckert, Mixed network former effects in tellurite glass systems: structure/property correlations in the system $(Na_2O)_{1/3}(2TeO_2)_x(P_2O_5)_{1-x})_{2/3}$, J. Phys. Chem. C 119 (2015) 17539–17551.

[14] A.C.M. Rodrigues, R. Keding, C. Rüssel, Mixed former effect between TeO_2 and SiO_2 in the Li_2O-TeO_2 -SiO_2 system, J. Non-Cryst. Solids 273 (2000) 53–58.

[15] M. Tatsumisago, K. Yoneda, N. Machida, T. Minami, Ionic conductivity of rapidly quenched glasses with high concentration of lithium ions, J. Non-Cryst. Solids 95–96 (1987) 857–864.

[16] S.P. Szu, C.T. Wu, Impedance study of 22.2Na_2O-(66.7-x)B_2O_3-xSiO_2 glasses, Mater. Chem. Phys. 100 (2006) 361–365.

[17] S.W. Martin, R. Christensen, G. Olson, J. Kieffer, W. Wang, New interpretation of Na^+-ion conduction in and the structures and properties of sodium borosilicate mixed glass former glasses, J. Phys. Chem. C 123 (2019) 5853–5870.

[18] A. Shaw, A. Ghosh, Dynamics of lithium ions in borotellurite mixed former glasses: correlation between the characteristic length scales of mobile ions and glass network structural units, J. Chem. Phys. 141 (2014) 164504.

[19] D. Larink, H. Eckert, Mixed network former effects in tellurite glass systems: structure/property correlations in the system $(Na_2O)_{1/3}(2(TeO_2)_x(B_2O_3)_{1-x})_{2/3}$, J. Non-Cryst. Solids 426 (2015) 150–158.

[20] M. de Oliveira, J. Schultz de Oliveira, S. Kundu, N.M. Pereira, A.C.M. Rodrigues, H. Eckert, Network former mixing effects in ion-conducting lithium borotellurite glasses: structure/property correlations in the system $(Li_2O)_y[2(TeO_2)_x(B_2O_3)_{1-x}]_{1-y}$, J. Non-Cryst. Solids 482 (2018) 14–22.

[21] L.F. Maia, A.C.M. Rodrigues, Electrical conductivity and relaxation frequency of lithium borosilicate glasses, Solid State Ion. 168 (2004) 87–92.

[22] S.M. Lee, Y.H. Kim, C.H. Song, S.J. Yoon, H.S. Kim, Y.S. Yang, Y.H. Rim, Dielectric and conduction behaviors of lithium germanium silicate glasses, J. Korean Phys. Soc. 58 (2011) 616–621.

[23] P. Balaya, P.S. Goyal, Non-Debye conductivity relaxation in a mixed glassformer system, J. Non-Cryst. Solids 351 (2005) 1573–1576.

[24] M. Schuch, C. Müller, P. Maass, S.W. Martin, Mixed barrier model for the mixed glass former effect in ion conducting glasses, Phys. Rev. Lett. 102 (2009) 145902.

[25] B. Deb, A. Ghosh, Correlation of macroscopic ion dynamics with microscopic length scale and modification of network structure in ion conducting mixed network former glasses, EPL 97 (2012) 16001.

[26] M.M. Smedskjaer, J.C. Mauro, Y. Yue, Cation diffusivity and the mixed network former effect in borosilicate glasses, J. Phys. Chem. B 119 (2015) 7106–7115.

[27] A. Palui, A. Ghosh, Structure-transport correlation of super-ionic mixed network former glasses, Solid State Ion. 343 (2019) 115126.

[28] A. Shaw, B. Deb, S. Kabi, A. Ghosh, Ion dynamics in single and mixed former glasses: correlation between microscopic lengths and network structure, J. Electroceram. 34 (2015) 20–27.

[29] T.D. Tho, R.P. Rao, S. Adams, Structure property correlation in lithium borophosphate glasses, Eur. Phys. J. E 35 (8) (2012) 1–11.

[30] M. Schuch, C. Trott, P. Maass, Network forming units in alkali borate and borophosphate glasses and the mixed glass former effect, RSC Adv. 1 (2011) 1370–1382.

[31] D. Zielniok, H. Eckert, C. Cramer, Direct correlation between nonrandom ion hopping and network structure in ion-conducting borophosphate glasses, Phys. Rev. Lett. 100 (2008) 035901.

[32] G. Tricot, Mixed network phosphate glasses: seeing beyond the 1D ^{31}P MAS-NMR spectra with 2D X/^{31}P NMR correlation maps, Ann. Rep. NMR Spectrosc. 96 (2019) 35–75.

[33] H. Eckert, Short and medium range order in ion conducting glasses studied by modern solid state NMR techniques, Z. Phys. Chem. 224 (2010) 1591–1653.

[34] R. Boehmer, K.R. Jeffrey, M. Vogel, Solid-state Li NMR with applications to the translational dynamics in ion conductors, Prog. Nucl. Magn. Reson. 50 (2007) 87–174.

[35] R.W. Schurko, Ultra-wideline NMR spectroscopy in solids, Acc. Chem. Res. 46 (2013) 1985–1995.

[36] L. O'Dell, The WURST kind of pulses in solid-state NMR, Solid State Nucl. Magn. Reson. 55 (2013) 28–41.

[37] D. Massiot, F. Fayon, M. Capron, I. King, S.L. Calvé, B. Alonso, J.O. Durand, B. Bujoli, Z. Gan, G. Hoatson, Modelling one- and two-dimensional solid-state NMR spectra, Magn. Reson. Chem. 40 (2002) 70–76.

[38] B. Gee, H. Eckert, ^{23}Na nuclear magnetic resonance spin echo decay spectroscopy of sodium silicate glasses and crystalline model compounds, Solid State Nucl. Magn. Reson. 5 (1995) 113–122.

[39] H. Verweij, J.H.J.M. Buster, The structure of lithium, sodium, and potassium germanate glasses, studied by Raman scattering, J. Non-Cryst. Solids 34 (1979) 81–99.

[40] J. Heo, D. Lam, G. Sigel, E. Mendoza, D. Hensley, Spectroscopic analysis of the structure and properties of alkali tellurite glasses, J. Am. Ceram. Soc. 75 (1992) 277–281.

[41] T. Sekiya, N. Mochida, A. Ohtsuka, M. Tonokawa, Raman spectra of $MO_{1/2}TeO_2$ (M = Li, Na, K, Rb, Cs) glasses, J. Non-Cryst. Solids 144 (1992) 128–144.

[42] R.T. Hart, U. Werner-Zwanziger, J.W. Zwanziger, On the spectral similarity of bridging and non-bridging oxygen in tellurites, J. Phys. Chem. A 109 (2005) 7636–7641.

[43] N.J. Boukharrata, P. Thomas, J.P. Laval, $GeTe_2O_6$, a germanium tellurate(IV) with an open framework, Acta Crystallogr. 65 (2009) i23–i26.

[44] J.B. D'Espinose de Lacaillerie, C. Fretigny, D. Massiot, MAS NMR spectra of quadrupolar nuclei in disordered solids: the Czjzek model, J. Magn. Reson. 192 (2008) 244–251.

[45] S.L. Tagg, R.E. Youngman, J.W. Zwanziger, The structure of sodium tellurite glasses: sodium cation environments from sodium-23 NMR, J. Phys. Chem. 99 (1995) 5111–5116.

[46] J.W. Zwanziger, J. Mc Laughlin, S.L. Tagg, Sodium distribution in sodium tellurite glasses probed by spin-echo NMR, Phys. Rev. B 56 (1997) 5243–5249.

[47] A. Larsson, D. Kuckling, M. Schönhoff, ^{1}H NMR of thermoreversible polymers in solution and at interfaces: the influence of charged groups on the phase transition, Colloids Surf. A Physicochem. Eng. Asp. 190 (2001) 185–192.

[48] J.S. Waugh, E.I. Fedin, Determination of hindered-rotation barriers in solids, Sov. Phys. Solid State 4 (1963) 1633–1636.

[49] L. Funke, H. Bradtmüller, H. Eckert, Recoupling dipolar interactions with multiple I = 1 quadrupolar nuclei: an ^{11}B{^{6}Li} and ^{31}P{^{6}Li} rotational echo double resonance study of lithium borophosphate glasses, Solid State Nucl. Magn. Reson. 84 (2017) 143–150.

[50] L. Funke, H. Eckert, Charge compensation in sodium borophosphate glasses studied by ^{11}B{^{23}Na} and ^{31}P{^{23}Na} rotational echo double resonance spectroscopy, J. Phys. Chem. C 120 (2016) 3196–3205.

[51] D. Larink, H. Eckert, M. Reichert, S.W. Martin, The mixed network former effect in ion-conducting alkali borophosphate glasses: structure/property correlations in the system $[M_2O]_{1/3}[(B_2O_3)_x(P_2O_5)_{1-x}]_{2/3}$ (M = Li, K, Cs), J. Phys. Chem. C 126 (2012) 26162–26176.